Since January 2020 Elsevier has created a COVID-19 resource centre with free information in English and Mandarin on the novel coronavirus COVID-19. The COVID-19 resource centre is hosted on Elsevier Connect, the company's public news and information website.

Virus Research 283 (2020) 197961

Contents lists available at ScienceDirect

Virus Research

journal homepage: www.elsevier.com/locate/virusres

Porcine deltacoronavirus activates the Raf/MEK/ERK pathway to promote its replication

Ji Hyun Jeon[a,1], Yoo Jin Lee[b,1], Changhee Lee[a,*]

[a] Animal Virology Laboratory, School of Life Sciences, BK21 plus KNU Creative BioResearch Group, Kyungpook National University, Daegu 41566, Republic of Korea
[b] Department of Neural Development and Disease, Korea Brain Research Institute, Daegu 41068, Republic of Korea

ARTICLE INFO

Keywords:
PDCoV
ERK1/2
Signal transduction
Cholesterol
Viral replication

ABSTRACT

Porcine deltacoronavirus (PDCoV) is a newly emerged swine coronavirus that causes acute enteritis in neonatal piglets. To date, little is known about the host factors or cellular signaling mechanisms associated with PDCoV replication. Since the Raf/MEK/ERK pathway is involved in modulation of various important cellular functions, numerous DNA and RNA viruses coopt this pathway for efficient propagation. In the present study, we found that PDCoV induces the activation of ERK1/2 and its downstream substrate Elk-1 early in infection irrespective of viral biosynthesis. Chemical inhibition or knockdown of ERK1/2 significantly suppressed viral replication, whereas treatment with an ERK activator increased viral yields. Direct pharmacological inhibition of ERK activation had no effect on the viral entry process but sequentially affected the post-entry steps of the virus life cycle. In addition, pharmacological sequestration of cellular or viral cholesterol downregulated PDCoV-induced ERK signaling, highlighting the significance of the cholesterol contents in ERK activation. However, ERK inhibition had no effect on PDCoV-triggered apoptosis through activation of the cytochrome c-mediated intrinsic mitochondrial pathway, suggesting the irrelevance of ERK activation to the apoptosis pathway during PDCoV infection. Altogether, our findings indicate that the ERK signaling pathway plays a pivotal role in viral biosynthesis to facilitate the optimal replication of PDCoV.

1. Introduction

Porcine deltacoronavirus (PDCoV) is a novel swine enteropathogenic coronavirus that causes acute diarrhea and vomiting in nursing piglets (Jung et al., 2015; Ma et al., 2015). Since its discovery in Hong Kong in 2012 (Woo et al., 2012), the virus has emerged in most parts of the world with industrialized pig production, threatening the swine industry worldwide (Lee and Lee, 2014; Li et al., 2014; Madapong et al., 2016; Marthaler et al., 2014; Saeng-Chuto et al., 2017; Song et al., 2015; Wang et al., 2015; Woo et al., 2012). PDCoV is a large, enveloped virus with a positive-stranded RNA genome of approximately 25.4 kb that belongs to the genus *Deltacoronavirus* within the family *Coronaviridae* of the order *Nidovirales* (Jung et al., 2015; Woo et al., 2012). The PDCoV genome is composed of a 5′ untranslated region (UTR), at least six open reading frames (ORF1a, ORF1b, and ORF2 through 5), and a 3′ UTR. The first two large ORF1a and 1b comprising the 5′ two-thirds of the genome encode two overlapping replicase polyproteins *via* a −1 ribosomal frameshift. Subsequent post-translational processing of the polyproteins by viral proteases results in 15 mature nonstructural proteins (nsp2–16). The remaining ORFs in the 3′-proximal region code for the four canonical coronaviral structural proteins, spike (S), membrane (M), envelope (E), and nucleocapsid (N), as well as three accessory proteins, nonstructural gene 6 (NS6), NS7, and NS7a (Fang et al., 2016, 2017; Lai et al., 2007; Lee and Lee, 2014; Li et al., 2014; Marthaler et al., 2014; Woo et al., 2012).

As viruses are limited in their genome size and coding capacity, they rely on a myriad of cellular factors or mechanisms to ensure coordinated replication. The mitogen-activated protein kinase (MAPK) pathways are central signaling networks that control a large number of principal cellular processes. The Raf/MEK/ERK signal transduction pathway is one of the MAPK cascades and comprises an array of three consecutive acting kinases: Raf, MEK1/2, and the extracellular signaling-regulated kinases 1 and 2 (ERK1/2). Upon various extracellular stimuli, this regulatory cascade event results in ERK1/2 activation, which phosphorylates numerous downstream substrates, leading to the transcription of multiple genes essential for diverse cellular functions,

* Corresponding author at: Animal Virology Laboratory, School of Life Sciences, College of Natural Sciences, Kyungpook National University, Daegu 41566, Republic of Korea.
E-mail address: changhee@knu.ac.kr (C. Lee).
[1] The authors contributed equally to this work and share co-first authorship.

https://doi.org/10.1016/j.virusres.2020.197961
Received 2 December 2019; Received in revised form 14 March 2020; Accepted 1 April 2020
Available online 10 April 2020
0168-1702/

such as cell proliferation, differentiation, survival or apoptosis (Diehl and Schaal, 2013; Gaur et al., 2010; Roux and Blenis, 2004; Shaul and Seger, 2007). Hence, it is not surprising that viruses hijack cellular signaling cascades, which in turn modulate and contribute to viral survival. Indeed, a number of viruses have been shown to inherit the Raf/MEK/ERK pathway to complete their replication cycle (Cai et al., 2007; Kim and Lee, 2015; Lee and Lee, 2010; Lim et al., 2005; Marjuki et al., 2006; Moser and Schultz-Cherry, 2008; Preugschas et al., 2019; Rodríguez et al., 2014; Schümann and Dobbelstein, 2006; Wang et al., 2006; Wei and Liu, 2009; Zampieri et al., 2007). However, the importance of the ERK signaling pathway in PDCoV replication has not been investigated thus far. Therefore, in this study, we aimed to examine whether PDCoV infection activates the ERK cascade in cultured cells and whether ERK activation is required for viral propagation.

2. Material and methods

2.1. Cells, virus, reagents, and antibodies

Swine testicular (ST) cells were cultured in alpha minimum essential medium (α-MEM; Invitrogen, Carlsbad, CA) with 5 % fetal bovine serum (FBS; Invitrogen) and antibiotic-antimycotic solutions (100×; Invitrogen). The cells were maintained at 37 °C in an atmosphere of humidified air containing 5 % CO_2. PDCoV strain KNU16-07 was propagated in ST cells in virus growth medium [α-MEM supplemented with antibiotic-antimycotic solutions, 10 mM HEPES (Invitrogen), and 5 μg/ml of trypsin (USB, Cleveland, OH)] without FBS as described previously (Jang et al., 2018). Mock-infected ST cells were also maintained under the same conditions with virus growth medium in the absence of FBS. The virus or mock inoculum stocks were prepared by freezing/thawing of virus-infected or un-infected ST cells, respectively, as described previously (Lee et al., 2015). Inactivation of PDCoV was performed by UV irradiation of the virus suspension with 1000 mJ/cm^2 using a UV crosslinker (Stratagene, La Jolla, CA). Virus inactivation was confirmed by the inoculation of the UV-treated virus on ST cells followed by N protein-specific staining as described below, and the inactivated virus was stored at −80 °C. The MEK1/2 inhibitors U0126 and PD98059, and ERK-specific and unconjugated control siRNAs were obtained from Cell Signaling Technology (Danvers, MA). Phorbol 12-myristate 13-acetate (PMA) and methyl-β-cyclodextrin (MβCD) were purchased from Sigma-Aldrich (St. Louis, MO). All reagents, except for MβCD, were dissolved in dimethyl sulfoxide (DMSO), while MβCD was prepared in distilled water. These compounds were diluted to the desired concentrations in maintenance medium and present during the entire period of virus or mock infection. The PDCoV N protein-specific monoclonal antibody (MAb) was described previously (Jang et al., 2018). Antibodies specific for ERK1/2, phosphorylated ERK1/2 (p-ERK1/2), and phosphorylated Elk-1 (p-Elk-1), were obtained from Cell Signaling Technology. The cytochrome *c* (cyt c), Bax, and β-actin antibodies and horseradish peroxidase (HRP)-conjugated goat anti-mouse or -rabbit IgG secondary antibodies were purchased from Santa Cruz Biotechnology (Santa Cruz, CA). Alexa Fluor 488-conjugated goat anti-mouse or -rabbit IgG and Alexa Flour 594-conjugated goat anti-mouse secondary antibodies and MitoTracker Red CMXRos (200 nM) were acquired from Invitrogen.

2.2. Cell viability assay

The cytotoxic effects of all reagents used in this study were analyzed using a colorimetric 3-(4,5-dimethylthiazol-2-yl)-2,5-diphenyltetrazolium bromide (MTT) assay (Sigma-Aldrich) to detect cell viability. Briefly, ST cells were grown at 1×10^4 cells/well in a 96-well tissue culture plate and treated with each chemical for 24 h. After 1 day of incubation, 50 μl of MTT solution (1.1 mg/ml) was added to each well, and the samples were incubated for an additional 4 h. The supernatant was then removed from each well, after which 150 μl of DMSO was added to dissolve the colored formazan crystals produced by the MTT. The absorbance of the solution was measured at 540 nm using an enzyme-linked immunosorbent assay plate reader. All MTT assays were performed in triplicate.

2.3. Western blot analysis and subcellular fractionation

ST cells were grown in 6-well tissue culture plates for 1 day and were mock infected or infected with PDCoV at a multiplicity of infection (MOI) or 1 or with an equal amount of UV-inactivated virus. At the indicated times, cells were harvested in 80 μl of lysis buffer (0.5 % TritonX-100, 60 mM β-glycerophosphate, 15 mM ρ-nitro phenyl phosphate, 25 mM MOPS, 15 mM $MgCl_2$, 80 mM NaCl, 15 mM EGTA [pH 7.4], 1 mM sodium orthovanadate, 1 μg/ml E64, 2 μg/ml aprotinin, 1 μg/ml leupeptin, and 1 mM PMSF) and sonicated on ice 5 times for 1 s each. Homogenates were lysed for 30 min on ice, and clarified by centrifugation at 15,800 × g (Eppendorf centrifuge 5415R, Hamburg, Germany) for 30 min at 4 °C. For subcellular fractionation, infectious or UV-inactivated PDCoV-infected ST cells were fractionated using a Nuclear/Cytosol Fractionation Kit (BioVision, Mountain View, CA). To investigate the effect of ERK inhibition or promotion on PDCoV replication, cells were independently pretreated with U0126 or PMA for 1 h and then infected with PDCoV at an MOI of 1. The virus-inoculated cells were further propagated in the presence of U0126 (50–100 μM), PMA (50–200 nM), or DMSO (0.5 %; vehicle control) and cell lysates were prepared with lysis buffer at 12 h post-infection (hpi). The total protein concentrations in the supernatants were determined using a BCA protein assay (Pierce, Rockford, IL). The cell lysates were mixed with 4× NuPAGE sample buffer (Invitrogen) and boiled at 70 °C for 10 min. Equal amounts of total protein were separated in a NuPAGE 4–12 % Gradient Bis-Tris Gel (Invitrogen) under reducing conditions and electrotransferred onto an Immobilon-P membrane (Millipore, Bedford, MA). The membranes were subsequently blocked with 3 % powdered skim milk (BD Biosciences, San Jose, CA) in TBS (10 mM Tris−HCl [pH 8.0], 150 mM NaCl) with 0.05 % Tween-20 (TBST) at 4 °C for 2 h and reacted at 4 °C overnight with the primary antibodies. The blots were then incubated with corresponding HRP-labeled secondary antibodies at a dilution of 1:5000 for 2 h at 4 °C. Finally, the proteins were visualized using enhanced chemiluminescence (ECL) reagents (GE Healthcare, Piscataway, NJ) according to the manufacturer' instructions. Ratios of phosphorylated/total ERK1/2, cytosolic/nuclear ERK1/2, and phosphorylated Elk-1/β-actin were compared by densitometry of the corresponding bands using a computer densitometry with the Wright Cell Imaging Facility (WCIF) version of the ImageJ software package (http://www.uhnresearch.ca/facilities/wcif/imagej/). To quantify viral protein production, band densities of the PDCoV N protein were quantitatively analyzed using a computer densitometer with ImageJ software based on the density value relative to the β-actin gene.

2.4. Fast activated cell-based ELISA (FACE)

FACE kit was obtained from Active Motif (Carlsbad, CA) and was used to determine the levels of ERK1/2 MAPK activation according to the manufacturer's protocols. Briefly, ST cells seeded in 96-well tissue culture plate were grown for 1 day and were infected with PDCoV or UV-inactivated virus as described above. At the indicated times, infected cells were fixed with 4 % formaldehyde. In addition, ST cells were pretreated independently with each MEK inhibitor for 1 h followed by PDCoV infection and fixed at 6 hpi. After washing and blocking, cells were reacted overnight with an anti-ERK1/2 or anti-phospho-ERK1/2 antibody. Following incubation with an HRP-conjugated secondary antibody, a colorimetric analysis was performed, with the absorbance of the solution determined at 450 nm using a spectrophotometer.

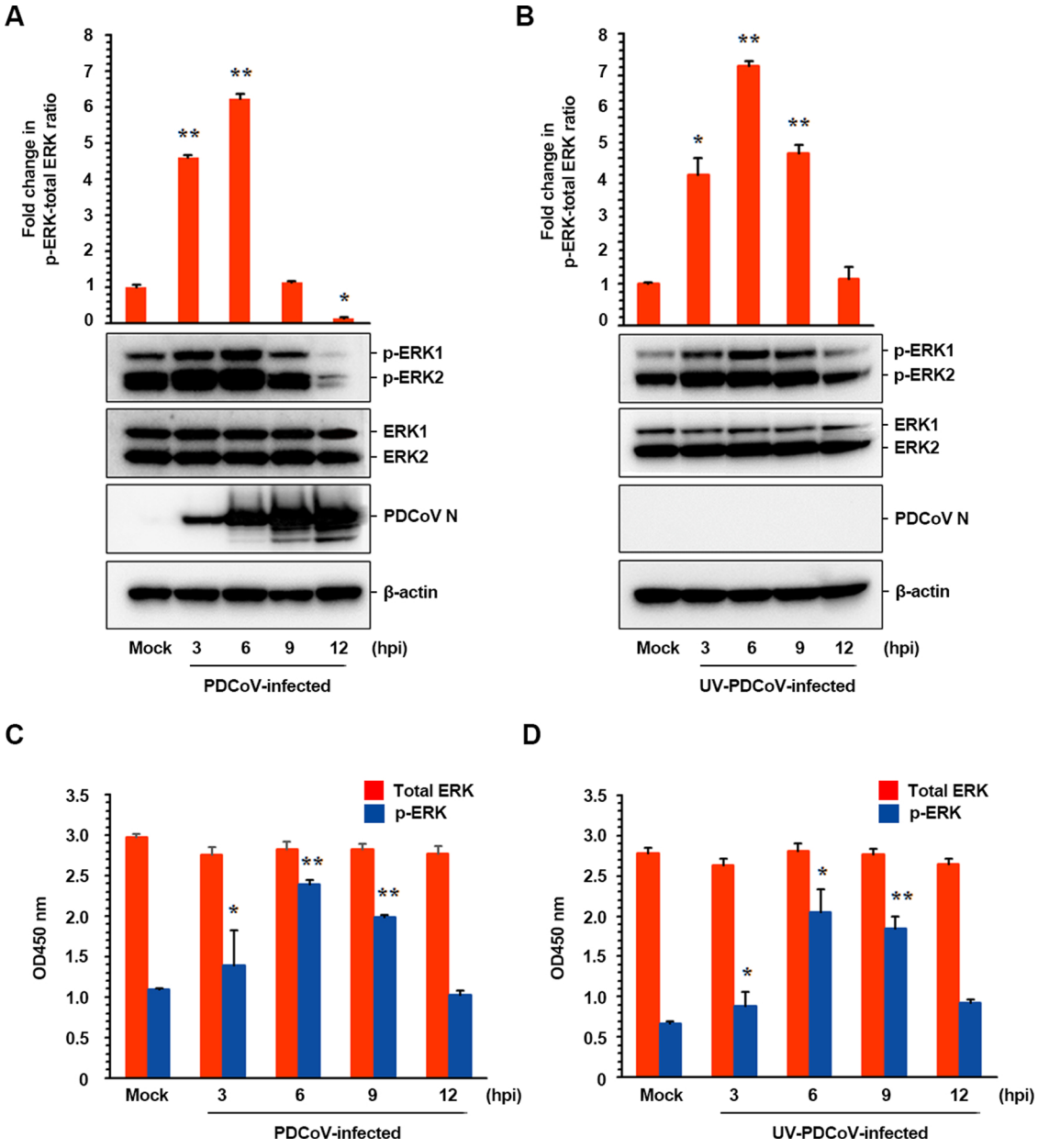

Fig. 1. PDCoV activates the ERK1/2 signaling pathway in cultured cells. ST cells were mock infected or infected with PDCoV at an MOI of 1 or an equal amount of UV-inactivated PDCoV. (A and B) Whole cell lysates were prepared for the indicated time points following infection and subjected to western blot analysis with the antibody specific for phosphorylated ERK1/2 (p-ERK1/2), ERK1/2, or the PDCoV N protein. The blot was also reacted with mouse MAb against β-actin to verify equal protein loading. Fold changes in the p-ERK1/2:total ERK1/2 ratio compared by densitometry of the corresponding bands using a computer densitometer are plotted. (C and D) ERK1/2 activation induced by PDCoV infection was quantitatively determined using a FACE assay. ST cells were fixed at the indicated time points with 4% formaldehyde and incubated with an anti-ERK1/2 or anti-p-ERK1/2 antibody followed by HRP-conjugated IgG antibodies. The absorbance of the solution was determined at 450 nm using a spectrophotometer. Data are the representative of the means from three independent experiments, and error bars denote the mean ± SDM. $*P < 0.05$; $**P < 0.001$.

2.5. Immunofluorescence assay (IFA)

ST cells grown on microscope coverslips placed in 6-well tissue culture plates were mock infected or infected with PDCoV or UV-inactivated PDCoV at an MOI of 1 for the indicated times. To assess the effect of MEK inhibitors on PDCoV infection, cells were pretreated with U0126, PD98059, or DMSO for 1 h and then infected with PDCoV. Virus-infected cells were subsequently maintained in the presence of vehicle or each inhibitor for 12 h. All treated cells were fixed with 4% paraformaldehyde for 10 min at room temperature (RT) and permeabilized with 0.2 % Triton X-100 in PBS at RT for 10 min. The cells were blocked using 1 % bovine serum albumin in PBS for 30 min at RT and then incubated with p-ERK1/2 and PDCoV N-specific antibodies or anti-N MAb for 2 h. After washing five times in PBS, the cells were incubated for 1 h at RT with corresponding Alexa Fluor-conjugated secondary antibodies, followed by counterstaining with 4′,6-diamidino-2-phenylindole (DAPI; Sigma-Aldrich). To examine subcellular localization of Bax and cyt c under the chemical inhibition of PDCoV-induced ERK activation, MitoTracker Red CMXRos was added to vehicle or MEK inhibitor-treated and virus-infected ST cells and left for 45 min at 37 °C prior to fixation. The cells were then stained with Bax- or cyt c-specific antibody as described above. The coverslips were mounted on glass microscope slides in mounting buffer and the stained cells were visualized using a Confocal Laser Scanning microscope (Carl Zeiss,

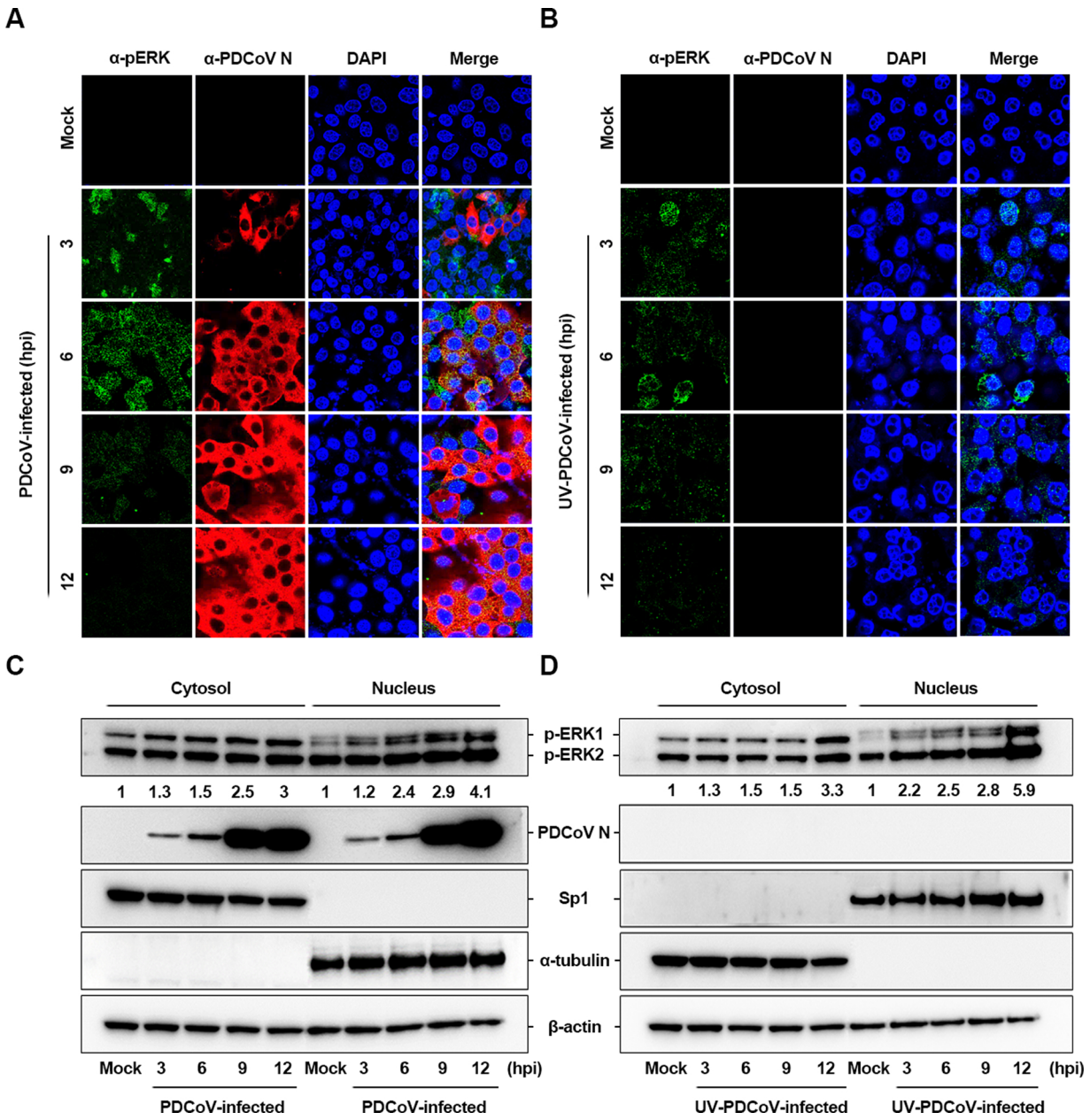

Fig. 2. PDCoV induces nuclear translocation of active ERK1/2. ST cells were mock infected or infected with PDCoV (A) or UV-inactivated PDCoV (B). At the indicated time points, infected cells were fixed and co-stained with antibodies against p-ERK1/2 (green) and PDCoV N (red). The cells were then counterstained with DAPI, and the intracellular localization of p-ERK1/2 in virus-infected cells was examined under a confocal microscope at 800× magnification. Western blot analysis of cell extracts infected with PDCoV (C) or UV-inactivated PDCoV (D). The cytosolic and nuclear fractions were prepared for the indicated time points and subjected to western blotting with an antibody directed against p-ERK (top panel), PDCoV N (second panel), Sp1 (nuclear protein marker; third panel), α-tubulin (cytosolic protein marker; fourth panel), or β-actin (bottom panel). All subcellular protein markers served as loading controls. The number under each band in the top panel represents fold changes in p-ERK level expressed as the densitometric unit of the band normalized to the corresponding loading control level as compared to the mock-infected control. Note that the presence of the PDCoV N protein in the nucleic fraction is shown as described previously (Lee and Lee, 2015).

Gattingen, Germany).

2.6. Fluorescence-activated cell sorting (FACS) analysis

Quantification of PDCoV-infected cells upon independent treatment of each reagent was analyzed using flow cytometry. ST cells were pretreated with each inhibitor or DMSO for 1 h, infected with PDCoV, and subsequently maintained in the presence of vehicle or each inhibitor. Virus-infected cells were trypsinized at 12 hpi and centrifuged at 250 × g (Hanil Centrifuge FLETA 5, Incheon, South Korea) for 5 min. The cell pellet was washed with cold washing buffer (1 % BSA and 0.1% sodium azide in PBS), and 10^6 cells were resuspended in 1 % formaldehyde solution in cold wash buffer for fixation at 4 °C in the dark for 30 min followed by centrifugation and incubation of the pellet in 0.2 % Triton X-100 in PBS at 37 °C for 15 min for permeabilization. After centrifugation, the cell pellet was resuspended in a solution of the primary anti-N MAb and the mixture was incubated at 4 °C for 30 min. The cells were washed and allowed to react with an Alexa Fluor 488-conjugated anti-mouse IgG secondary antibody at 4 °C for 30 min in the dark. The stained cells were washed again and analyzed using a FACSAria III flow cytometer (BD Biosciences).

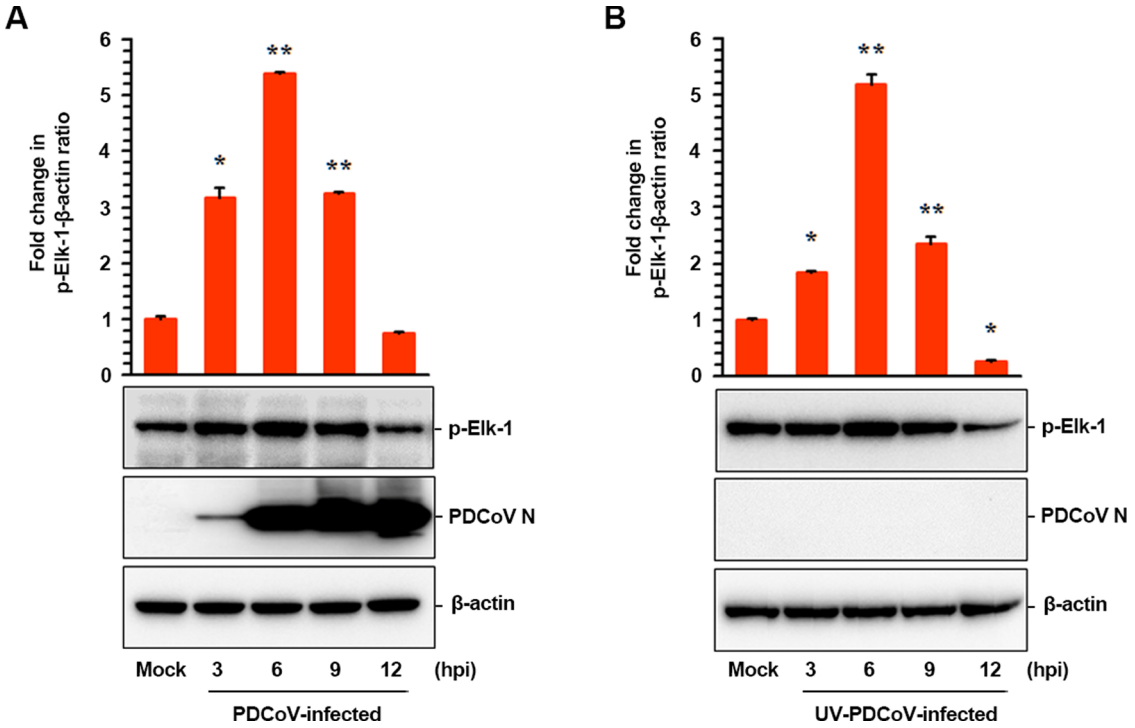

Fig. 3. Phosphorylated ERK1/2 leads to the activation of downstream target Elk-1. ST cells were mock infected or infected with PDCoV at an MOI of 1 (A) or an equal amount of UV-inactivated PDCoV (B). Whole cell lysates were prepared for the indicated time points following infection and subjected to western blot analysis with the antibody to p-Elk-1 or PDCoV N. The blot was also reacted with mouse MAb against β-actin to verify equal protein loading. Fold changes in the p-Elk-1:β-actin ratio are plotted. Results are the representative of the means from three independent experiments, and error bars denote the mean ± SDM. $^{*}P < 0.05$; $^{**}P < 0.001$.

2.7. Time course of MEK1/2 inhibitor treatment

ST cells were infected with PDCoV at an MOI of 1. At −1, 0, 1, 2, 4, 6, 8, 10, or 12 hpi, U0126 was added to give the indicated final concentration over the remainder of the time course experiment. The PDCoV-infected and inhibitor-treated cells were further maintained and trypsinized at 12 hpi, followed by centrifugation. The harvested cells were subjected to FACS analysis to assess the magnitude of PDCoV infection as described above.

2.8. Knocked down expression of ERK by siRNA

ST cells were transfected with 100 nM siRNA targeting ERK1/2 or control siRNA using Lipofectamine 3000 (Invitrogen) according to the manufacturer's protocols. At 24 h post-transfection, cells were infected with PDCoV at an MOI of 1 for 12 h. ERK1/2 proteins were detected by western blot analysis and quantitatively analyzed using a computer densitometer as described above. At 12 hpi, the infected cells were subjected to PDCoV N-specific IFA or FACS analysis as described above, while the culture supernatants were harvested and subjected to virus titration as described below.

2.9. Virus titration

ST cells were infected with PDCoV and treated with each chemical or DMSO in duplicate as described above. The culture supernatant was collected from each well at different time points (3, 6, 9, 12, and 24 hpi) and stored at −80 °C. The PDCoV titer was measured by limiting dilution on ST cells in duplicate as described previously (Jang et al., 2018), and then 50 % tissue culture infectious dose ($TCID_{50}$) per ml was calculated using Reed-Muench method (Reed and Muench, 1938).

2.10. Virus binding and internalization assays

Binding and internalization assays were performed as described previously with some modifications (Cai et al., 2007). ST cells grown in 6-well culture plates were pretreated and infected with PDCoV at an MOI of 1 at 4 °C for 1 h in the presence of U0126. Unbound viruses were then removed by washing with PBS, and the cells were either incubated at 4 °C (allowing virus binding only) or 37 °C (permitting virus binding and internalization) in the presence of U0126 for 1 h. In the latter case, the cells were further treated with proteinase K (0.5 mg/ml) at 37 °C for 45 min to remove bound but uninternalized virus particles. The PDCoV-infected cells were then serially diluted in α-MEM medium and inoculated onto fresh ST cell monolayers in 96-well tissue culture plates. At 24 h post-incubation, bound or internalized viruses were titrated by IFA as described above, and the $TCID_{50}$ was determined.

2.11. Quantitative real-time RT-PCR

ST cells were incubated with U0126 or DMSO for 1 h prior to infection and then inoculated with PDCoV at an MOI of 1 for 1 h at 37 °C. The virus inoculum was subsequently removed, and the infected cells were maintained in fresh medium containing U0126 or DMSO for 12 h. Total RNA was extracted from lysates of the infected cells at 12 hpi using the TRIzol Reagent (Invitrogen) and was treated with DNase I (TaKaRa, Otsu, Japan) according to the manufacturer's instructions. The concentrations of extracted RNA were measured using a NanoVue spectrophotometer (GE Healthcare, Piscataway, NJ). Quantitative real-time RT-PCR was performed using a Thermal Cycler Dice Real-Time System (TaKaRa) with gene-specific primer sets as described previously (Kim and Lee, 2013). The RNA levels of viral genes were normalized to that of mRNA for the β-actin, and the relative quantities (RQ) of mRNA accumulation were calculated using the $2^{-\Delta\Delta Ct}$ method (Livak and Schmittgen, 2001). To detect alterations in the genomic RNA and sg

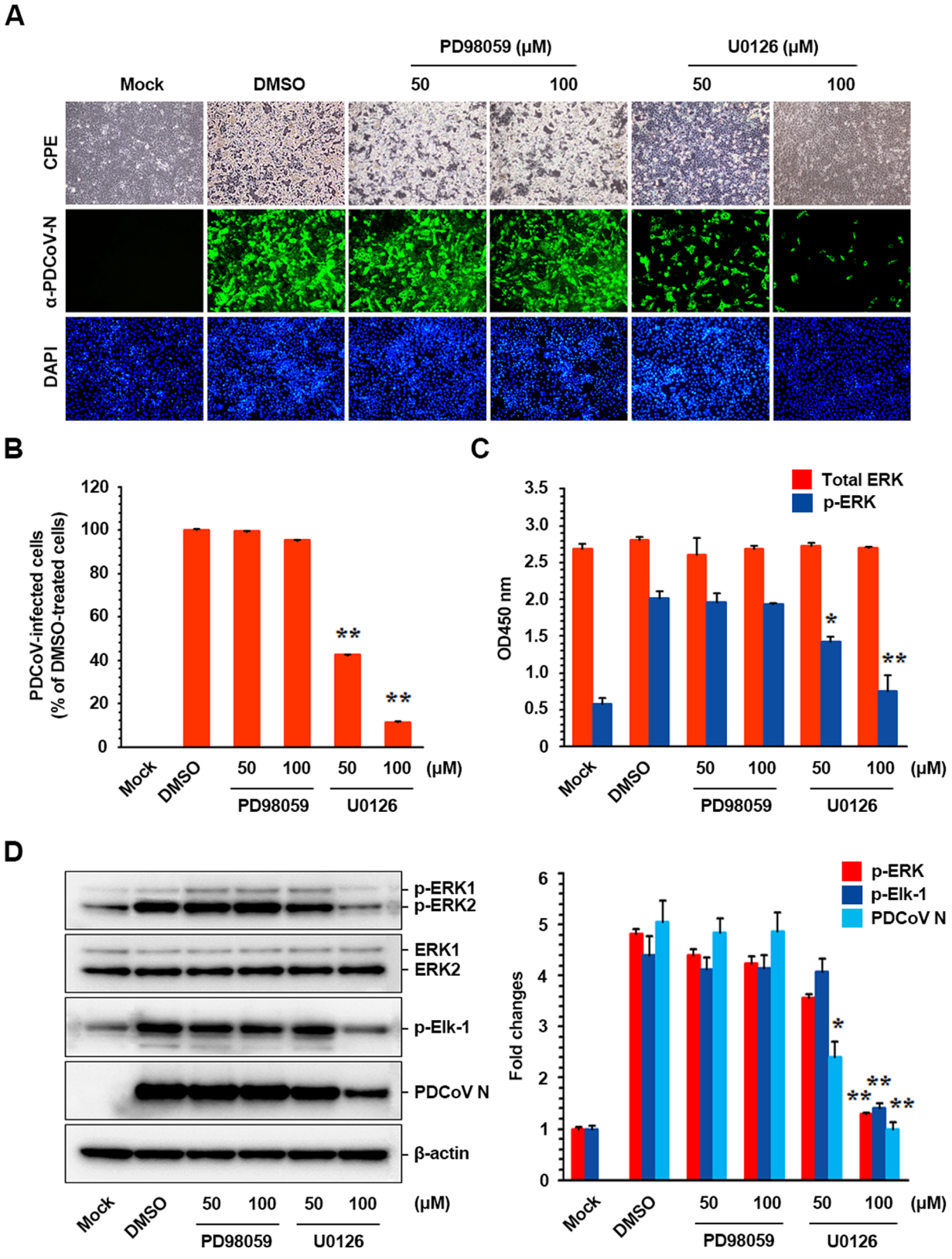

(caption on next page)

mRNA levels in the presence of U0126 during PDCoV infection, the results obtained using inhibitor-treated cells were compared to those from DMSO-treated cells.

2.12. Depletion of cholesterol from the cell or virus

ST cells were pretreated with MβCD at various concentrations for 1 h and then inoculated with PDCoV at an MOI of 1 for 1 h. The virus-infected cells were the grown in the presence of MβCD for 6 h. In

Fig. 4. Inhibition of ERK1/2 activation impairs PDCoV propagation. (A) ST cells were preincubated with DMSO, PD98059 (50 and 100 μM), or U0126 (50 and 100 μM) for 1 h prior to infection and were mock infected or infected with PDCoV at an MOI of 1. The virus-infected cells were further maintained for 12 h in the presence of DMSO or inhibitors. PDCoV-specific CPEs were monitored and photographed at 12 hpi under an inverted microscope at the magnification of 200× (first panels). For immunostaining, the infected cells were fixed at 12 hpi and incubated with MAb against the PDCoV N protein, followed by incubation with Alexa green-conjugated goat anti-mouse secondary antibody (second panels). The cells were then counterstained with DAPI (third panels) and examined under a fluorescent microscope at 200× magnification. (B) PDCoV production in the presence of each inhibitor was quantified by measuring the percentage of cells expressing N proteins through flow cytometry. (C) Chemical inhibition of ERK1/2 was quantitatively determined using a FACE assay. ST cells were mock infected or PDCoV infected in the presence of DMSO, PD98059, or U0126. The cells were fixed at 6 hpi with 4% formaldehyde and incubated with an anti-ERK1/2 or anti-phospho-ERK1/2 antibody followed by HRP-conjugated IgG antibodies. The absorbance of the solution was determined at 450 nm using a spectrophotometer. (D) At 6 hpi, cellular lysates were prepared and subjected to immunoblotting using an antibody against p-ERK1/2, ERK1/2, p-Elk-1, or PDCoV N. The blot was also reacted with an anti-β-actin antibody to verify equal protein leading. Each protein expression was quantitatively analyzed by densitometry, and fold changes in each p-ERK1/2:total ERK1/2, p-Elk-1:β-actin, and PDCoV N:β-actin ratio are independently plotted (right panel). Data are the representative of the means from three independent experiments, and error bars denote the mean ± SDM. *P < 0.05; **P < 0.001.

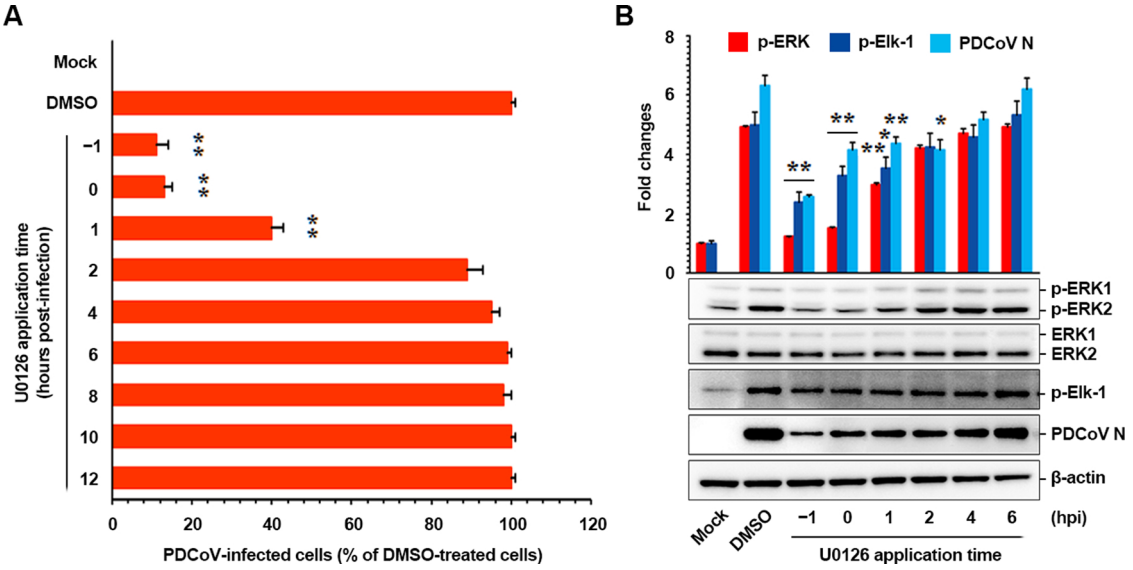

Fig. 5. Chemical inhibitor of ERK1/2 is present at the early stage to inhibit virus production. (A) ST cells were pretreated with DMSO or U0126 (100 μM) and mock or PDCoV (MOI of 1) infected. At the indicated time points post-infection, U0126 was added to achieve the intended final concentration. At 12 hpi, virus-infected cells were trypsinized, and virus infectivity was determined by measuring the percentage of cells expressing N proteins through FACS. (B) Whole cell lysates were prepared for the indicated time points of U0126 treatment and subjected to western blot analysis with the antibody to p-ERK1/2, ERK1/2, p-Elk-1, or PDCoV N. The blot was also reacted with an anti-β-actin antibody to verify equal protein leading. Each protein expression was quantitatively analyzed by densitometry, and fold changes in each p-ERK1/2:total ERK1/2, p-Elk-1:β-actin, and PDCoV N:β-actin ratio are independently plotted. Results are presented as the mean values of three independent experiments, and error bars denote the mean ± SDM. *P < 0.05; **P < 0.001.

addition, PDCoV was treated with MβCD at 37 °C for 1 h followed by ultracentrifugation to remove the MβCD as descried previously, and the purified virus was used to infect ST cells (Jeon and Lee, 2017). At 6 hpi, the culture supernatants were collected, while the infected cells were fixed with 4 % formaldehyde. The samples were independently subjected to virus titration and a FACE assay as described above. In parallel, the cellular or viral cholesterol content was determined using a Cholesterol Cell-Based Detection Assay Kit (Cayman Chemical, Ann Arbor, MI) as descried previously (Jeon and Lee, 2017).

2.13. Annexin V and PI staining assay

ST cells were pretreated with U0126 and then mock infected or infected with PDCoV at an MOI of 1. The virus-inoculated cells were further propagated in the presence of U0126 (100 μM) or DMSO. Phosphatidylserine exposure was determined by measuring Annexin V binding at the indicated times using an Alexa Fluor 488 Annexin V/Dead Cell Apoptosis kit (Invitrogen), according to the manufacturer's protocols. In brief, cells were harvested, washed with cold PBS, and suspended in 100 μl 1× annexin-binding buffer. The cells were then incubated with Alexa Fluor 488-conjugated Annexin V and propidium iodide (PI) at RT for 15 min in the dark. Following the incubation period, 400 μl of annexin-binding buffer was added to each sample, and the samples were mixed gently and kept on ice. The fluorescent signals of Annexin V and PI were detected at channels FL-1 and FL-2, respectively, and analyzed using a BD FACSAria III flow cytometer. Cells negative for PI uptake and positive for Annexin V were considered apoptotic.

2.14. Statistical analysis

All values are expressed as the mean ± standard deviation of the mean (SDM). Statistical analyses were performed using Student's t test. P-values of less than 0.05 were considered to be statistically significant.

3. Results

3.1. PDCoV activates ERK1/2

To investigate the activation status of the ERK1/2 signaling cascade during PDCoV replication, the kinetics of ERK1/2 phosphorylation in ST cells infected with PDCoV at an MOI of 1 were monitored at different times post-infection using western blot analysis. As shown in Fig. 1A, activated ERK1/2 was detected in mock-infected ST cells and this was considered the background level of phosphorylated ERK1/2 (p-ERK1/2) that is likely responsive to the components of the culture media. In contrast, PDCoV infection significantly increased ERK1/2 activity by 3 hpi, with a peak at 6 hpi, reversal to the background levels at 9 hpi, and

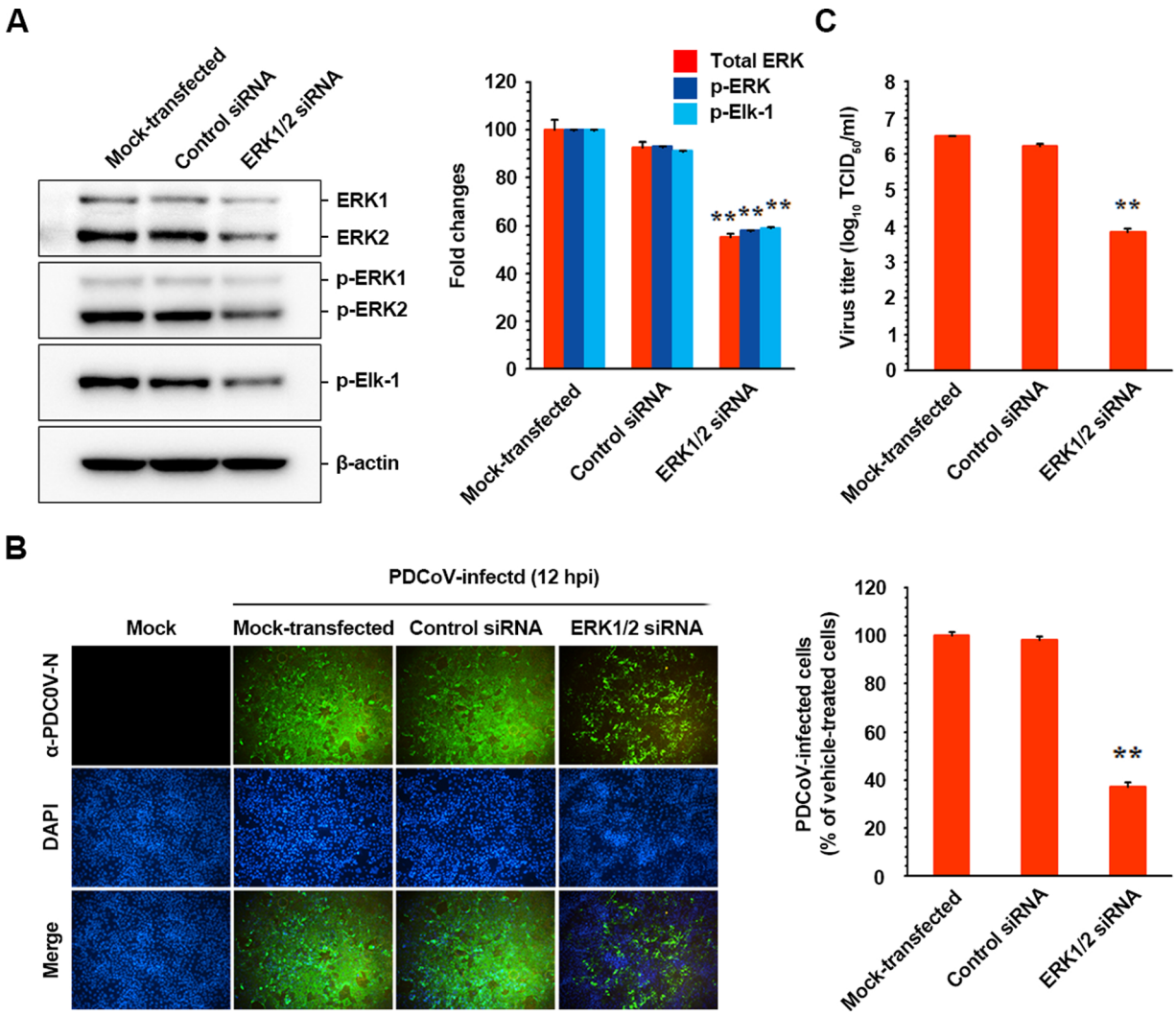

Fig. 6. ERK1/2 knockdown suppresses PDCoV infection. (A) ST cells were transfected with 100 nM ERK-specific siRNA or control siRNA using Lipofectamine 3000 followed by PDCoV infection at 24 h post-transfection. At 12 hpi, cellular lysates were prepared and subjected to immunoblotting using an antibody against ERK1/2, p-ERK1/2, or p-Elk-1. The blot was also reacted with an anti-β-actin antibody to verify equal protein leading. Each protein expression was quantitatively analyzed by densitometry and presented as the relative density value to the β-actin gene, and fold changes in each protein:β-actin ratio are plotted. (B) For immunostaining, transfected and infected cells were fixed at 12 hpi and stained with an anti-PDCoV N antibody followed by Alexa green-conjugated goat anti-mouse secondary antibody (first panels). The cells were then counterstained with DAPI (second panels) and examined under a fluorescent microscope at 200× magnification. Quantification of PDCoV production was assessed exactly as described in the legend of Fig. 4B and presented (left panel) (C) The virus supernatants were collected at 12 hpi, and viral titers were determined. Values are representative of the mean of three independent experiments, and error bars represent the mean ± SDM. $^{**}P < 0.001$.

a dramatic decrease thereafter (Fig. 1A). In addition, the activation profile of ERK1/2 was comparably dynamic in cells infected with PDCoV at an MOI of 0.1 (data not shown). These results indicated that PDCoV infection triggers early strong but temporary activation of ERK1/2. Since ERK1/2 phosphorylation did not steadily increase with ongoing replication, it was assumed that ERK1/2 activation occurred independent of the considerable protein production obvious at later time points. To confirm this hypothesis, we used UV-irradiated inactivated PDCoV, which can bind to and internalize into target cells but cannot replicate upon infection. UV-inactivated PDCoV was able to sufficiently stimulate ERK1/2 activation with similar kinetics as that observed in PDCoV-infected cells (Fig. 1B). These data indicate that virion attachment to host cells is responsible for monophasic ERK activation.

Next, we attempted to confirm the activation levels of ERK1/2 in cells infected with PDCoV or UV-inactivated PDCoV using a FACE assay. Likewise, the most significant increase in the ERK1/2 phosphorylation occurred at 6 h after PDCoV infection (Fig. 1C). Moreover, the activation patterns of ERK1/2 in the UV-irradiated PDCoV-exposed cells were nearly identical to those in the non-irradiated PDCoV-infected cells (Fig. 1D). In addition, the levels of total ERK1/2 remained unchanged in the cells infected with both normal and inactivated PDCoV at various time points after infection when compared to those in mock-infected cells. Taken together, our results demonstrated that ERK activation occurs in a monophasic manner during PDCoV infection and is unnecessary for viral replication.

3.2. PDCoV translocates p-ERK1/2 into the nucleus and phosphorylates Elk-1

Upon activation, ERK molecules are translocated into the nucleus, where they phosphorylate a variety of transcription factors. The subcellular localization of p-ERK1/2 was examined in cells infected with PDCoV and UV-inactivated PDCoV (Fig. 2). In mock-infected cells, no active ERK1/2 was evident in any cellular compartments during the entire experiment (Fig. 2A and B, top panels). In contrast, the nuclear

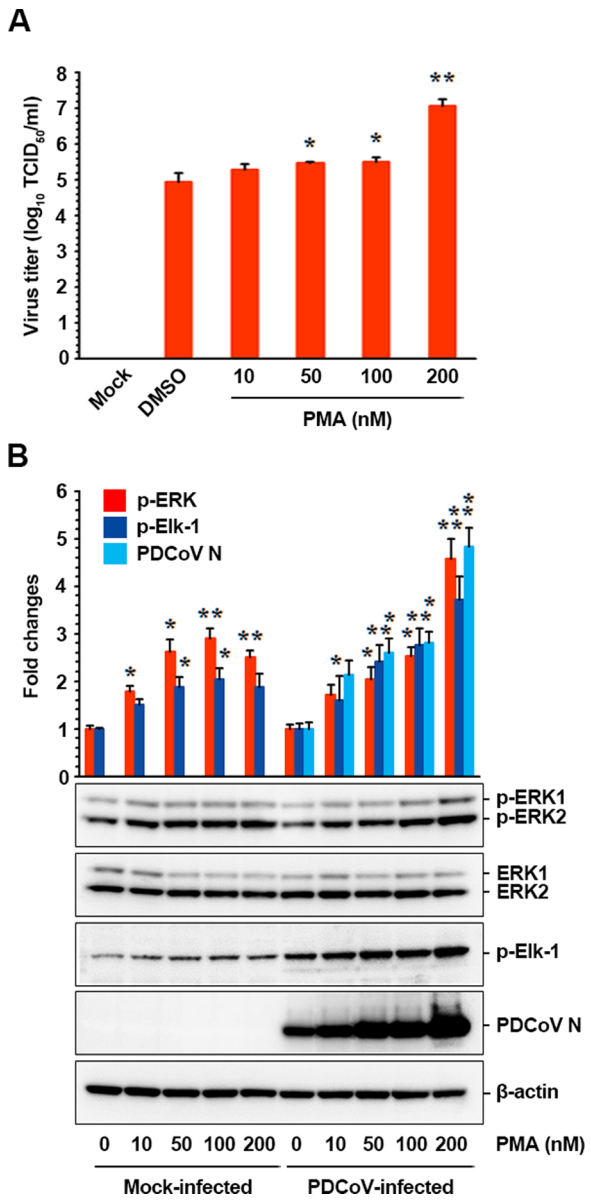

Fig. 7. Pharmacological activation enhances PDCoV multiplication. (A) ST cells were mock or PDCoV infected (MOI of 1) for 1 h and then maintained in fresh medium containing DMSO or various concentrations of PMA. At 6 hpi, the virus supernatants were collected, and virus titers were determined. (B) Whole cell lysates were prepared at 6 hpi and subjected to western blot analysis with the antibody specific for p-ERK1/2, ERK1/2, p-Elk-1, or PDCoV N. The blot was also reacted with an anti β-actin antibody to verify equal protein loading. Fold changes in each p-ERK1/2:total ERK1/2, p-Elk-1:β-actin, and PDCoV N:β-actin ratio are independently plotted. Values shown are representative of the mean of three independent experiments, and error bars denote the mean ± SDM. $^{*}P < 0.05$; $^{**}P < 0.001$.

punctate distribution of p-ERK1/2 was observed at 3 hpi and continuously confirmed up to 9 hpi (Fig. 2A). Comparably, after exposure of cells to UV-inactivated PDCoV, p-ERK1/2 was scattered in the nucleus and cytoplasm. The punctate localization pattern of active ERK molecules persisted for 9 h after treatment with inactivated PDCoV (Fig. 2B). These observations were confirmed by Western blot analysis with cytosolic and nuclear extracts of PDCoV-infected cells (Fig. 2C and D). Considering that the transcription factor Elk-1 is downstream of ERK and its activity is regulated by ERK-dependent phosphorylation (Wei and Liu, 2009), we investigated the activation status of Elk-1 following PDCoV-induced ERK activation (Fig. 3). PDCoV infection augmented the amount of phosphorylated Elk-1 with kinetics that indistinguishably coincided with those observed in ERK1/2 activation (Fig. 3A). Likewise, phosphorylated Elk-1 components increased in cells treated with UV-inactivated PDCoV, comparable to the increase in PDCoV-infected cells (Fig. 3B). These findings indicated that ERK signaling activated by PDCoV infection regulates downstream effector molecules that control the expression of target genes crucial for inducible cellular processes.

3.3. ERK1/2 activation regulates PDCoV replication

To assess the biological effects of ERK1/2 activation on PDCoV infection, virological assays were conducted in the presence or absence of specific inhibitors of the ERK signaling pathway. ST cells were pretreated with the MEK1/2 inhibitor U0126 or PD98059 at concentrations of 50 and 100 μM or with DMSO (0.5 %) as a vehicle control for 1 h prior to infection. The inhibitors and DMSO were present during the entire period of infection. The results of an MTT assay revealed that none of the inhibitor doses tested in the present study affected the cell viability (data not shown). Viral production was assessed by monitoring the strength of the CPE and confirmed by immunofluorescence using N protein-specific MAb at 12 hpi (Fig. 4A). Vehicle-treated control cells exhibited distinct CPE and PDCoV N protein-specific staining in many cell clusters, indicating infection and the spread of the virus to neighboring cells. Similarly, virus propagation was clearly observed in the presence of PD98059 at all concentrations examined, indicating no detrimental effect on PDCoV replication. However, the inhibitory effect of U0126 on virus infection was readily detectable. As shown in Fig. 4A, U0126 significantly suppressed PDCoV-induced CPE (first panels) and PDCoV gene expression (second panels) in a dose-dependent manner. Quantification of N protein staining results showed that the proportion (%) of virus-infected cells was only reduced upon U0126 treatment, leading to nearly 90 % inhibition at the highest concentration tested (Fig. 4B). To further verify relevance, we determined the activation status of ERK1/2 using a FACE assay after treatment with the two inhibitors in PDCoV-infected cells. PD98059 did not affect PDCoV-induced ERK activation, whereas U0126 markedly declined the levels of p-ERK1/2 (Fig. 4C). The specificity and effectiveness of each inhibitor on PDCoV infection-induced phosphorylation of ERK and its downstream target Elk-1 were confirmed by Western blot analysis (Fig. 4D). Taken together, these data demonstrated that the MEK inhibitor hampered ERK and Elk-1 activation and accordingly attenuated PDCoV propagation, indicating a virtual role of ERK1/2 as cellular factors for PDCoV infection. We used U0126 in all subsequent experiments due to its significant inhibitory effect on PDCoV replication.

To determine the point at which the MEK inhibitor acts during PDCoV infection, ST cells were treated with U0126 at various time points post-infection. At 12 hpi, the levels of PDCoV replication were quantified indirectly by measuring cells expressing viral N proteins using flow cytometry (Fig. 5A). The addition of 100 μM U0126 up to 1 hpi resulted in inhibitory effects on PDCoV production compared to the levels in the DMSO-added control. Treating cells with U0126 at −1 and 0 hpi resulted in an approximately 90 % decrease, while treatment at 1 hpi caused a 60 % reduction in viral infectivity. However, no significant inhibition in PDCoV propagation was identified when the compound was added after 1 hpi. In addition, treatment of cells with U0126 up to 1 hpi caused a significant diminution in ERK and Elk-1 activation in PDCoV-infected cells, which are corresponding to the decrease of virus production at the indicated time points of chemical application (Fig. 5B). These results corroborated that U0126 must be present at the adsorption stage of viral infection to exert its inhibitory effect on PDCoV replication by suppressing ERK activation. This finding further indicates that the pre-entry period of PDCoV infection is sufficient for the activation of the ERK signaling pathway.

To directly corroborate the involvement of the Raf/MEK/ERK pathway in PDCoV multiplication, we investigated the effect of ERK

silencing on viral production. ST cells were transfected with ERK-specific siRNA or a nonspecific siRNA as a negative control. At 24 h post-transfection, cells were infected with PDCoV, and the amounts of target gene expression and virus propagation were quantified at 12 hpi (Fig. 6). Transfection of cells with ERK-specific siRNA resulted in a nearly 50% inhibition of the expression of ERK as well as Elk-1 compared to the levels in mock transfected or in those transfected with the control siRNA (Fig. 6A). ERK silencing caused a more than 60 % decrease in the expression of the PDCoV N protein and an over 2-log reduction in virus yields compared to the mock- or nonspecific siRNA-transfected controls (B and C). These data showed that specific knockdown of ERK1/2 impairs virus propagation, demonstrating the essential participation of ERK in PDCoV replication.

Several extracellular factors including phorbol esters such as PMA are known to activate ERK (Abkhezr et al., 2010). To examine the effect of PMA on PDCoV propagation, cells inoculated with PDCoV for 1 h were incubated with culture medium containing a vehicle or different concentrations of PMA and virus production was measured at 6 hpi. A more than 2-log enhancement in virus titer was obtained at the highest concentration used (Fig. 7A). A significant augmentation in ERK and Elk-1 phosphorylation was observed in mock- and PDCoV-infected cells treated with increasing concentrations of PMA (Fig. 7B). Furthermore, PMA treatment noticeably upregulated the expression of PDCoV N protein in a dose-dependent manner (Fig. 7B), which correlates with the increase of virus yields and supports the idea that PMA promotes PDCoV replication by activating the ERK pathway.

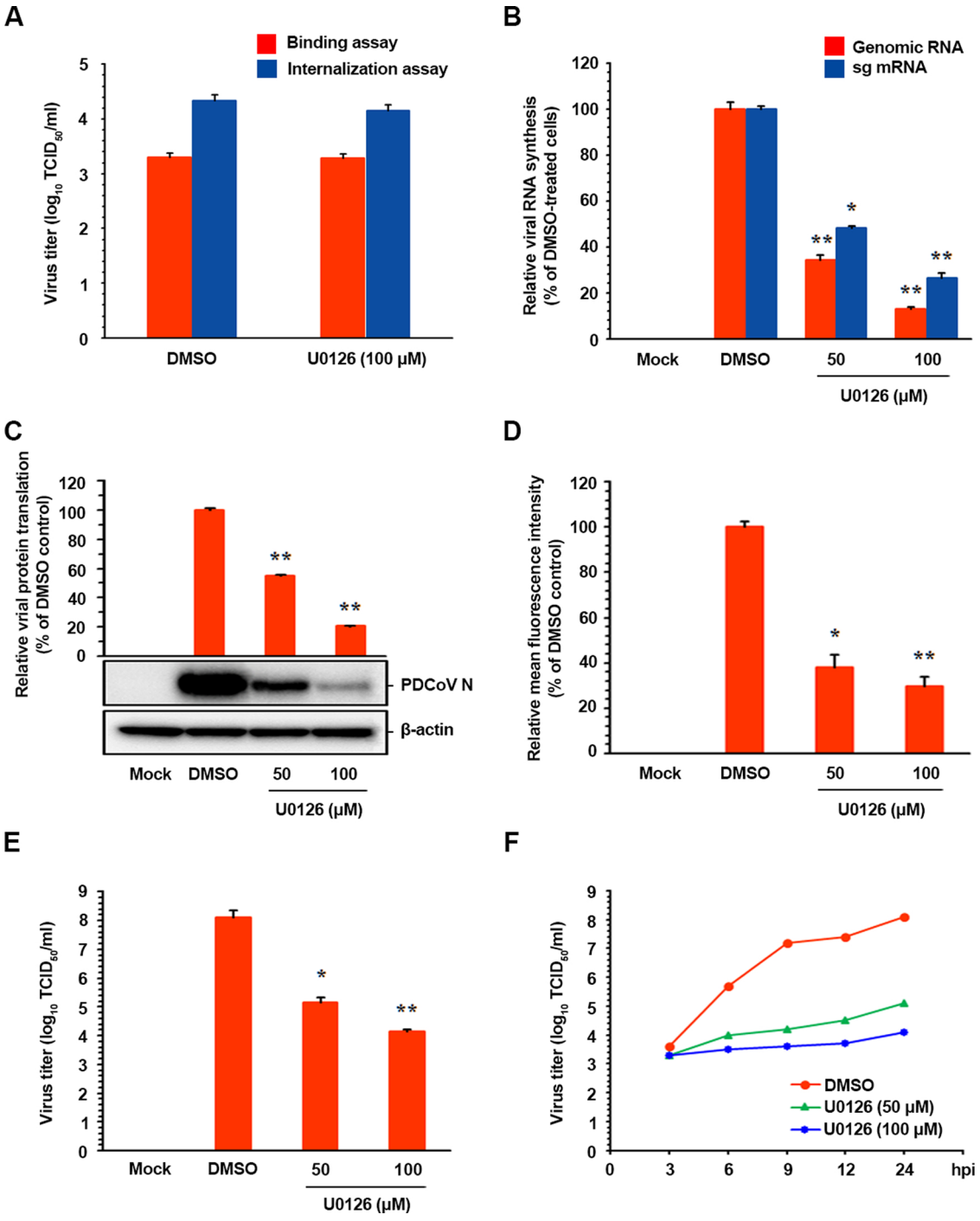

(caption on next page)

Fig. 8. Pharmacological inhibition of ERK1/2 activation has no effect on virus entry but interferes with each post-entry step of PDCoV replication. (A) Effect of ERK inhibition on virus binding and internalization. ST cells were infected with PDCoV at an MOI of 1 at 4 °C for 1 h. After washing with cold PBS, infected cells were maintained in the presence or absence of U0126, either at 4 °C (red bars) or 37 °C (blue bars) for an additional hour. The virus-infected cells maintained at 37 °C were further treated with proteinase K at 37 °C. The infected cells were then serially diluted and plated onto fresh ST cells. At 24 h post-incubation, internalized viruses were titrated by IFA. (B) Effect of ERK inhibition on viral RNA synthesis. ST cells pretreated with DMSO or U0126 were mock infected or infected with PDCoV (MOI of 1) for 1 h and then incubated in either DMSO or U0126. Total cellular RNA was extracted at 12 hpi, and strand-specific viral genomic RNAs (red bars) and sg mRNAs (blue bars) of PDCoV were amplified by quantitative real-time RT-PCR. Viral positive-sense genomic RNA and sg mRNA levels were normalized to those of porcine β-actin, and relative quantities (RQ) of accumulated mRNA were determined. The results obtained with U0126-treated samples were compared with those obtained with DMSO-treated samples. (C) Effect of ERK inhibition on viral protein translation. U0126-treated ST cells were mock infected or infected with PDCoV for 1 h and further cultivated in the presence or absence of U0126. At 12 hpi, cellular lysates were prepared, resolved by SDS-PAGE, transferred to a nitrocellulose membrane, and immunoblotted using the antibody against the PDCoV N protein. The blot was also reacted with an anti β-actin antibody to verify equal protein loading. Viral protein expression was quantitatively estimated by densitometry and presented as the density value relative to that of the β-actin gene. U0126-treated sample results were compared to those of the vehicle control. (D) Effect of ERK inhibition on the intensity of viral protein expression. Under the same experimental conditions as in panel C, the PDCoV-infected cells were trypsinized at 12 hpi and subjected to FACS analysis using an anti-PDCoV N antibody to determine the mean fluorescence intensity. The results of U0126-treated samples were compared to those of DMSO-treated control. (E) Effect of ERK inhibition on viral progeny production. ST cells were pretreated with DMSO or U0126 for 1 h and were mock or PDCoV infected (MOI of 1). Vehicle or U0126 was present in the medium throughout the infection. At 24 hpi, virus-containing culture supernatants were collected, and PDCoV titers were determined. (F) Effect of ERK inhibition on viral growth kinetics. PDCoV reproduction after treatment with U0126 was assessed exactly as in panel A. At the indicated time points post-infection, culture supernatants were harvested and virus titers were measured. Results are expressed as the mean values of three independent experiments, and error bars represent standard deviations. $*P < 0.05$; $**P < 0.001$.

3.4. Pharmacological inhibition of ERK1/2 activation has no effect on the virus entry process but impairs the post-entry steps of the PDCoV replication cycle

Next, we aimed to pinpoint the step(s) in the multiplication cycle of PDCoV targeted by the inhibition of ERK activation. To address this issue, the earliest steps, specifically the two stages of virus entry (attachment and penetration), were assessed using an internalization assay after treatment with the MEK inhibitor. ST cells were inoculated with PDCoV at 4 °C for 1 h to allow only virus attachment and were further maintained either at 4 °C or 37 °C to limit or permit virus internalization, respectively, in the presence of U0126. The cells incubated at 37 °C were subsequently treated with proteinase K to remove remnant virus particles from the cell surface. Serially diluted infected cells were then subjected to an infectious center assay on uninfected ST cell monolayers, and virus titers were measured (Fig. 8A). The cells maintained at 4 °C to permit virus binding while preventing internalization produced infectious virus particles irrespective of the presence of U0126, likely due to incomplete removal of the bound viruses. Moreover, the viral titers were equivalent in cells treated with U0126 or vehicle incubated at 37 °C to allow virus penetration to proceed. These results indicated that U0126 has no inhibitory effects on the virus entry process.

As with other coronaviruses, virus entry leads to the release of the PDCoV genome into the cytoplasm where the genomic RNA directly serves as a template for early gene expression by exploiting the host translation machinery, immediately producing polyproteins, which are proteolytically processed into nsps. The nonstructural replicase proteins subsequently drive *de novo* synthesis of two viral RNA entities: genomic and subgenomic (sg) RNAs. The sg mRNA transcripts are translated late in the cycle to their respective structural proteins. Therefore, to investigate the functional mechanism of ERK1/2 regulation of PDCoV infection in the post-entry phases, we first tested whether the inhibition of ERK1/2 activation exclusively affected genome replication and sg mRNA transcription. To accomplish this, the relative levels of both genomic RNA and sg mRNA were measured using quantitative real-time strand-specific RT-PCR in the presence or absence of U0126 following PDCoV infection. As shown in Fig. 8B, U0126 greatly diminished the synthesis of PDCoV genomic RNA and sg mRNA in a dose-dependent manner compared to that in DMSO-treated infected cells. The decreases in viral RNA levels after the addition of U0126 did not reflect non-specific inhibition of transcription because the mRNA levels of the internal β-actin control remained unchanged in all samples (data not shown).

Since ERK inhibition negatively regulates the expression of PDCoV genomic RNA and sg mRNA, it may further suppress the viral protein production resulting from cascade-like inhibition of viral RNA synthesis. Thus, we examined whether viral protein translation was affected by ERK inhibition. For this approach, ST cells were exposed to U0126 for 1 h prior to infection, and the compound was present during infection and subsequent incubation. The expression level of the PDCoV N

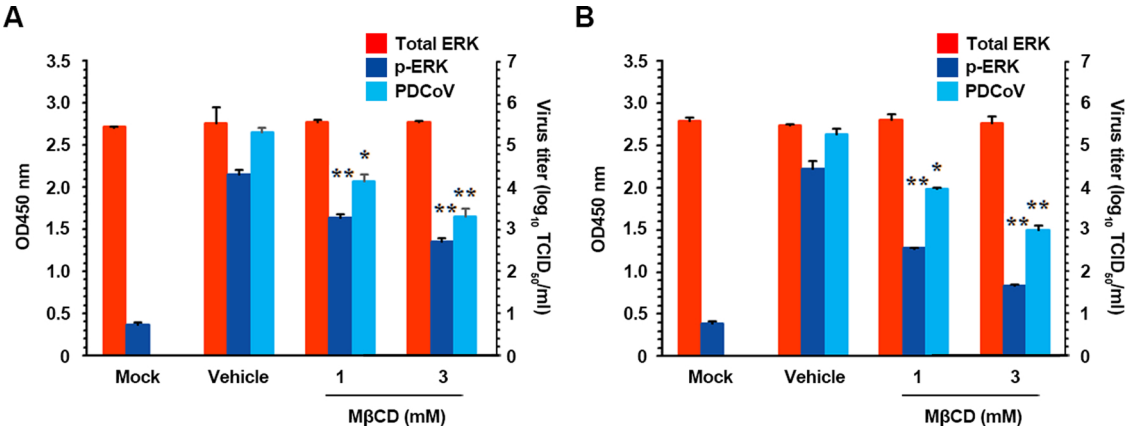

Fig. 9. Depletion of cellular or viral cholesterol modulates PDCoV-induced ERK activation. Effects of cholesterol sequestration after treatment of cells (A) or virions (B) with MβCD (1 and 3 mM) on PDCoV-induced ERK activation and viral progeny production were quantitatively determined at 6 hpi using a FACE assay and virus titration under the same experimental conditions as in Figs. 4C and 8E, respectively. Values are representative of the mean from three independent experiments, and error bars denote the mean ± SDM. $*P < 0.05$; $**P < 0.001$.

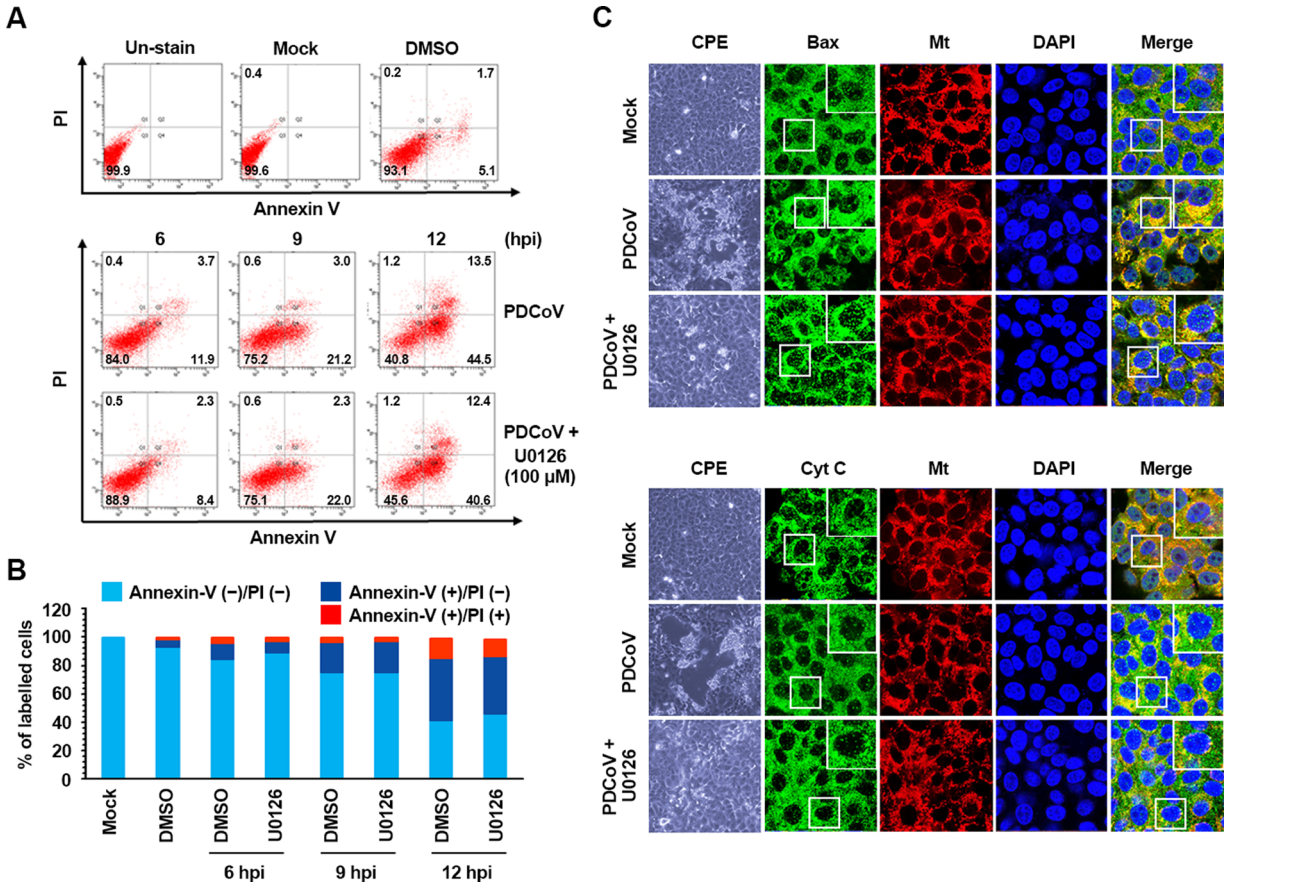

Fig. 10. Inhibition of ERK1/2 activation does not influence PDCoV-induced apoptosis. (A) ST cells were treated with DMSO or U0126 (100 μM) for 1 h prior to infection and then mock infected or infected with PDCoV in the presence of DMSO or U0126. The cells harvested at the indicated time points were subjected to dual Annexin V and PI labeling and analyzed by FACS. Lower left quadrants represent intact cells (Annexin V negative/PI negative); Lower right quadrants represent early apoptotic cells (Annexin V positive/PI negative); Upper right quadrants indicate late apoptotic or/and necrotic cells (Annexin V positive/PI positive); and Upper left quadrants indicate necrotic cells (Annexin V negative/PI positive). The figure is representative of three independent experiments. (B) The graph represents the percentage of each quadrant, and the non-significant percentages of Annexin V-negative and PI-positive cells were excluded. (C) The U0126-treated and infected cells were labeled with MitoTracker Red CMXRos (red), fixed at 12 hpi, and independently incubated with a primary antibody against Bax or cyt c (green). The cells were then counterstained with DAPI and examined under a confocal microscope at 800× magnification. PDCoV-specific CPEs were also photographed at 12 hpi under an inverted microscope at the magnification of 200× (left panels). Bax mitochondrial translocation is represented as the merger of Bax and mitochondrial marker (yellow), while the residual cytosolic localization is indicated by single staining signal (green). Conversely, cyt c cytosolic translocation is represented by single staining signal (green), and residual mitochondrial accumulation is indicated as the merger of cyt c and MitoTracker (yellow). The inset images are enlarged versions of parts of the picture.

protein in the presence of U0126 or DMSO was evaluated at 12 hpi using western blot analysis. Pharmacological inhibition had a detrimental effect on viral protein production at different concentrations (Fig. 8C). Densitometric analysis of the western blots revealed that the N protein expression was dramatically downregulated by U0126, with a maximum of 80% inhibition at the highest concentration. Moreover, comparable lessened kinetics in the mean fluorescence intensity corresponding to PDCoV N protein production was confirmed in the presence of the inhibitor (Fig. 8D). These data demonstrated the suppressive effect of the ERK inhibitor on viral protein expression due to its specific upstream action on viral RNA biosynthesis during PDCoV replication.

In addition, virus yields were determined during treatment with the MEK inhibitor to assess whether ERK activity is necessary for the production of infectious viral progeny. Upon infection, viral supernatants were collected at 24 hpi and viral titers were measured. As illustrated in Fig. 8E, the presence of U0126 reduced the release of viral progeny in a dose-dependent manner. The peak viral titer was determined to be $10^{8.1}$ $TCID_{50}$/ml in the vehicle-treated control. However, the addition of 100 μM U0126 declined the PDCoV titer to $10^{4.15}$ $TCID_{50}$/ml (a nearly 4-log reduction compared to the control level). The growth kinetics study also indicated substantial attenuation of PDCoV replication, reflecting the diminished process of viral biosynthesis when cells were treated with U0126 (Fig. 8F). These findings confirmed that ERK1/2 activation is integral to optimal progeny virus production from host cells.

3.5. Both cellular and virion cholesterols contribute to ERK1/2 activation

The disruption of lipid rafts by the depletion cholesterol has been shown to result in the inhibition of ERK activation, suggesting a potential effect of cholesterol on ERK signaling (Sorice et al., 2008; Yan et al., 2012). Since PDCoV infection requires cholesterol present in both the cell membrane and the viral envelope (Jeon and Lee, 2018), it was rational to investigate whether cholesterol plays a role in PDCoV-induced ERK activation. To answer this question, we employed MβCD, which is the most common cholesterol-sequestering agent used for plasma membranes. To examine the importance of cellular cholesterol in ERK activation, ST cells were pretreated with MβCD at various concentrations or with ethanol as a vehicle control for 1 h prior to infection and the compound or vehicle was present throughout infection. Based on the MTT assay results, none of the MβCD doses tested in the

present study caused detectable levels of cell death (data not shown). The activation levels of ERK1/2 upon MβCD treatment were measured with a FACE assay. As shown in Fig. 9A, the addition of a cholesterol-depleting compound to the target cells significantly diminished virus-induced ERK phosphorylation as well as PDCoV replication compared to that in the vehicle-treated control upon infection in a dose-dependent manner. To investigate the effect of cholesterol depletion in the viral envelope on ERK signaling, PDCoV was treated with 1 or 3 mM MβCD prior to inoculation. Likewise, the removal of cholesterol from virions resulted in a significant decrease in the amounts of activated ERK1/2 and PDCoV production (Fig. 9B). In addition, we assured the ability of MβCD to deplete the cellular or virion cholesterol contents after treatment using a fluorescent filipin III staining (data not shown). Taken together, our data indicated the involvement of cholesterols maintained in the cell and viral membranes in the ERK signaling pathway.

3.6. ERK1/2 activation is irrelevant to PDCoV-induced apoptosis

The Raf/MEK/ERK signaling pathway orchestrates numerous cellular processes including pro- and anti-proliferative events depending on stressors. Accumulating evidence suggests that ERK activity is associated with apoptosis execution under certain conditions (Cagnol and Chambard, 2010). Intriguingly, PDCoV can induce caspase-dependent apoptosis through activation of the cytochrome *c* (cyt c)-mediated intrinsic mitochondrial pathway, thereby facilitating viral replication *in vitro* (Lee and Lee, 2018). Considering our previous findings, we anticipated that the ERK cascade may function in the induction of apoptosis by PDCoV infection. Thus, we initially assessed the effect of ERK inhibition on PDCoV-triggered apoptosis using Annexin V/PI flow cytometry. ST cells were treated with DMSO or U0126 and then infected with PDCoV. At various time points post-infection, the treated and infected cells were stained with Annexin V and PI and examined with FACS analysis to quantitatively measure the percentage of viable, apoptotic, and dead cells (Fig. 10A). Neither the vehicle nor the inhibitor tested caused significant apoptosis under our experimental conditions (top panels). Consistent with our previous study (Lee and Lee, 2018), PDCoV infection in the presence of DMSO produced a significant level of apoptosis (Annexin V positive/PI negative) at 6 hpi, and the percentage of early apoptotic cells progressively increased with infection time (middle panels). Nonetheless, pharmacological inhibition of ERK1/2 activity failed to protect the cells from PDCoV-induced apoptotic death (bottom panels). The fraction of early apoptosis in cells treated with U0126 was comparable to that in vehicle-treated cells during the course of PDCoV infection (Fig. 10B). Furthermore, both cytosolic-to-mitochondrial translocation of Bax and mitochondrial-to-cytosolic release of cyt c, hallmarks of PDCoV-mediated apoptosis, remained unaffected in the presence of the ERK inhibitor (Lee and Lee, 2018; Fig. 10C). Taken together, our data indicated that the ERK signaling pathway is unrelated to PDCoV-triggered apoptosis and its mechanism.

4. Discussion

The understanding of the interplay between the virus and host signaling pathways has been extensively studied. In particular, the ERK cascade plays multiple significant roles in a variety of cellular functions that control cell destination, which in turn, can govern viruses that rely entirely on the host cell machinery to survive. Thus, viruses have evolved to devise general methods to take advantage of ERK signaling that benefits the viral replication machinery for optimal virus infection. However, no information is unveiled regarding the intracellular signaling pathways involved in PDCoV replication. The current study demonstrated for the first time that ERK activation is essential for the optimal replication of PDCoV in cultured cells. In this study, we found that PDCoV induces early strong and transient activation of ERK1/2 independent of maximal viral production, indicating the significance of the ERK cascade for PDCoV infection. Chemical inhibition and specific knockdown of ERK1/2 greatly impaired PDCoV propagation. Moreover, pharmacological inhibition of ERK activation extensively suppressed viral multiplication, particularly affecting the post-entry stages, as determined by the global down-regulation of viral RNA synthesis, viral protein expression, and progeny release. Therefore, PDCoV was shown to manipulate the ERK signaling pathway to ensure competent viral biosynthesis and reproduction in target cells.

Analogous to infectious PDCoV, the UV-inactivated virus efficiently stimulated the phosphorylation of ERK and its downstream target with comparable activation profiles; therefore, ERK signaling was awakened independent of virus replication but dependent on virus entry events such as virus-receptor interaction and uncoating. Moreover, the upmost growth of PDCoV commenced at 9 hpi, as determined by the detection of a maximal amount of the viral protein, corresponding to the time when the activated status of ERK1/2 returned to the basal level or below. In contrast, total ERK1/2 levels remained steady in cells throughout infection with non-irradiated or UV-irradiated PDCoV. Altogether, the negligible production of PDCoV infection within 6 hpi is satisfactory for maximal activation of the ERK signaling pathway. These observations were comparably reproduced in porcine IPEC-J2 intestinal epithelial cells infected with infectious or UV-inactivated PDCoV, indicating that PDCoV-induced ERK signaling is cell type independent (Supplementary Fig. S1). Interestingly, other nidoviruses trigger similar ERK1/2 activation kinetics that occurs in response to virus entry, suggesting a unique feature of the ERK pathway in the nidovirus biology (Cai et al., 2007; Kim and Lee, 2015; Lee and Lee, 2010). Although the present study did not uncover an exact mean to evoke ERK signaling following PDCoV infection, it is tempting to speculate that extracellular viruses bound to the receptor are likely responsible for ERK activation. However, we cannot exclude the activation of ERK cascades by other stimuli, including incoming virus particles through direct fusion or disassembled viral proteins and the released genome after the uncoating process.

In this study, two MEK inhibitors, PD98059 and U0126, were employed to investigate the favorable contributions of ERK signaling to the replication of PDCoV. However, PD98059 failed to deliver the expected results, showing no suppressive effects on both ERK activation and viral propagation. This differentiating effect of each inhibitor on PDCoV replication was further corroborated in IPEC-J2 cells infected with PDCoV upon compound treatment (Supplementary Fig. S2). PD98059 prevents ERK1/2 activation by blocking the phosphorylation of MEK1/2, whereas U0126 is capable of not only averting the activation of MEK1/2 but also inhibiting MEK1/2 activity (Alessi et al., 1995; Davis et al., 2000). Therefore, U0126 is known to be a more potent inhibitor of ERK1/2 activation than PD98059 (Favata et al., 1998). Our findings support the distinguished ability of PD98059 and U0126 to suppress ERK1/2 phosphorylation, which correlated with their different effects on PDCoV production. However, we previously demonstrated that the two inhibitors independently hindered ERK activation induced by the porcine epidemic diarrhea virus (PEDV), another swine enteric coronavirus, and accordingly, potently impaired PEDV replication (Kim and Lee, 2015). Considering previous and current findings, PDCoV replication seems to be less reliant on the magnitude of ERK activation than PEDV, indicating that the ERK dependence of infection differs among coronaviruses.

Given the knowledge gained from the present study, a feasible elucidation of how ERK1/2 activation controls PDCoV infection is that the ERK pathway may positively regulate viral multiplication directly or indirectly. Inhibition of PDCoV-provoked ERK activation remarkably waned each post-adsorption step of the viral replication process, including viral biosynthesis and subsequent release. Growing evidence indicates that the viral RNA polymerases, also called RNA-dependent RNA polymerases (RdRps), of positive-sense RNA viruses are phosphoproteins activated by host protein kinases, such as ERK1/2,

suggesting a regulatory role of RdRp phosphorylation in viral RNA replication (Jakubiec and Jupin, 2007; Moser and Schultz-Cherry, 2008). Thus, ERK1/2 activity may be crucial to phosphorylate and stabilize the PDCoV RdRp (nsp12), which could be a prerequisite for optimal viral RNA biosynthesis and later replication steps. In addition, we previously found that both cellular and viral cholesterols are key players in the entry process of PDCoV (Jeon and Lee, 2018). Contrary to the previous study, however, despite the influence of PDCoV-induced ERK activation by cellular or virion cholesterols, the ERK signaling pathway is irrelevant to both virus attachment and internalization. These observations led us to hypothesize that the cholesterol itself present in either the cell membrane or viral envelope, rather than cholesterol-dependent viral entry, acts as a stimulus to activate the ERK signaling pathway upon PDCoV infection. On the other hand, the ERK signaling pathway is involved in both intrinsic and extrinsic apoptotic pathways by triggering mitochondrial cyt c release or caspase-8 activation, respectively (Cagnol and Chambard, 2010). Several viruses can mediate apoptosis by activating the ERK cascade and thereby, promote their replication (Wong et al., 2005; Zampieri et al., 2007). Although PDCoV infection is known to induce caspase-dependent intrinsic apoptosis *in vitro* to favor viral replication (Lee and Lee, 2018), the current study showed no crosstalk between ERK1/2 activation and apoptosis during PDCoV infection. This finding was unanticipated because specific relocation of the mitochondrial cyt c into the cytoplasm primarily participated in the PDCoV-triggered apoptosis pathway (Lee and Lee, 2018). However, PDCoV can induce apoptotic cell death and cause the release of apoptogenic cyt c irrespective of ERK signaling, suggestive of the engagement of other host mechanisms, such as other MAPK pathways. Alternatively, ERK1/2 activation may be indirectly involved in PDCoV infection through cross-talk with other cascades to regulate the advent of other host factors that may necessitate maximal viral propagation. Furthermore, our trials on pharmacological inhibition consistently reduced but never completely eliminated PDCoV infectivity, indicating the presence of additional intracellular elements or machineries simultaneously hijacked by the invaded virus to ensure the productive survival and spread of the virus.

In conclusion, our findings revealed that PDCoV activates ERK1/2 in the early period of virus infection in cultured cells and the activated ERK molecules are required for competent PDCoV replication *in vitro*. However, the exact viral processes and constituents responsible for ERK activation remain undetermined. Although our data demonstrated the suppression of viral RNA and consequent protein biosynthesis following the inhibition of ERK activation, the specific mechanism by which PDCoV-activated ERK signaling modulates the viral replication cycle during infection is uncertain. Since a better understanding of the precise function of ERK activation in PDCoV multiplication will provide valuable insights into the molecular biology and pathogenesis of the virus, elucidating the mechanism will become an important aspect of our future studies.

CRediT authorship contribution statement

Ji Hyun Jeon: Methodology, Software, Validation, Investigation, Data curation, Formal analysis, Writing - original draft, Visualization. **Yoo Jin Lee:** Methodology, Software, Validation, Investigation, Data curation, Formal analysis, Writing - original draft, Visualization. **Changhee Lee:** Conceptualization, Methodology, Validation, Supervision, Writing - review & editing.

Declaration of Competing Interest

The authors declare that they have no conflict of interest.

Acknowledgments

This research was supported by the Basic Science Research Programs through the National Research Foundation of Korea (NRF) funded by the Ministry of Education (NRF-2015R1D1A1A09057406 and NRF-2017M3C7A1048089).

Appendix A. Supplementary data

Supplementary material related to this article can be found, in the online version, at doi:https://doi.org/10.1016/j.virusres.2020.197961.

References

Abkhezr, M., Keramati, A.R., Ostad, S.N., Davoodi, J., Ghahremani, M.H., 2010. The time course of Akt and ERK activation on XIAP expression in HEK 293 cell line. Mol. Biol. Rep. 37, 2037–2042.
Alessi, D.R., Cuenda, A., Cohen, P., Dudley, D.T., Saltiel, A.R., 1995. PD 098059 is a specific inhibitor of the activation of mitogen-activated protein kinase kinase *in vitro* and *in vivo*. J. Biol. Chem. 270, 27489–27494.
Cagnol, S., Chambard, J.C., 2010. ERK and cell death: mechanisms of ERK-induced cell death-apoptosis, autophagy and senescence. FEBS J. 277, 2–21.
Cai, Y., Liu, Y., Zhang, X., 2007. Suppression of coronavirus replication by inhibition of the MEK signaling pathway. J. Virol. 81, 446–456.
Davis, S., Vanhoutte, P., Pages, C., Caboche, J., Laroche, S., 2000. The MAPK/ERK cascade targets both Elk-1 and cAMP response element-binding protein to control long-term potentiation-dependent gene expression in the dentate gyrus *in vivo*. J. Neurosci. 20, 4563–4572.
Diehl, N., Schaal, H., 2013. Make yourself at home: viral hijacking of the PI3K/Akt signaling pathway. Viruses 5, 3192–3212.
Fang, P., Fang, L., Hong, Y., Liu, X., Dong, N., Ma, P., Bi, J., Wang, D., Xiao, S., 2017. Discovery of a novel accessory protein NS7a encoded by porcine deltacoronavirus. J. Gen. Virol. 98, 173–178.
Fang, P., Fang, L., Liu, X., Hong, Y., Wang, Y., Dong, N., Ma, P., Bi, J., Wang, D., Xiao, S., 2016. Identification and subcellular localization of porcine deltacoronavirus accessory protein NS6. Virology 499, 170–177.
Favata, M.F., Horiuchi, K.Y., Manos, E.J., Daulerio, A.J., Stradley, D.A., Feeser, W.S., Van Dyk, D.E., Pitts, W.J., Earl, R.A., Hobbs, F., Copeland, R.A., Magolda, R.L., Scherle, P.A., Trzaskos, J.M., 1998. Identification of a novel inhibitor of mitogen-activated protein kinase kinase. J. Biol. Chem. 273, 18623–18632.
Gaur, P., Munjhal, A., Lal, S.K., 2010. Influenza virus and cell signaling pathways. Med. Sci. Monit. 17, RA148–154.
Jakubiec, A., Jupin, I., 2007. Regulation of positive-strand RNA virus replication: the emerging role of phosphorylation. Virus Res. 129, 73–79.
Jang, G., Kim, S.H., Lee, Y.J., Kim, S., Lee, D.S., Lee, K.K., Lee, C., 2018. Isolation and characterization of a korean porcine deltacoronavirus strain KNU16-07. J. Vet. Sci. 19, 577–581.
Jeon, J.H., Lee, C., 2017. Cellular cholesterol is required for porcine nidovirus infection. Arch. Virol. 162, 3753–3767.
Jeon, J.H., Lee, C., 2018. Cholesterol is important for the entry process of porcine deltacoronavirus. Arch. Virol. 163, 3119–3124.
Jung, K., Hu, H., Eyerly, B., Lu, Z., Chepngeno, J., Saif, L.J., 2015. Pathogenicity of 2 porcine deltacoronavirus strains in gnotobiotic pigs. Emerg. Infect. Dis. 21, 650–654.
Kim, Y., Lee, C., 2013. Ribavirin efficiently suppresses porcine nidovirus replication. Virus Res. 171, 44–53.
Kim, Y., Lee, C., 2015. Extracellular signal-regulated kinase (ERK) activation is required for porcine epidemic diarrhea virus replication. Virology 484, 181–193.
Lai, M.C., Perlman, S., Anderson, L.J., 2007. Coronaviridae. In: Knipe, D.M., Howley, P.M., Griffin, D.E., Martin, M.A., Lamb, R.A., Roizman, B., Straus, S.E. (Eds.), Fields Virology, 5th ed. Lippincott Williams & Wilkins., Philadelphia, PA, pp. 1305–1336.
Lee, S., Kim, Y., Lee, C., 2015. Isolation and characterization of a Korean porcine epidemic diarrhea virus strain KNU-141112. Virus Res. 208, 215–224.
Lee, S., Lee, C., 2014. Complete genome characterization of Korean porcine deltacoronavirus strain KOR/KNU14-04/2014. Genome Announc. 2, e01191–14.
Lee, S., Lee, C., 2015. Functional characterization and proteomic analysis of the nucleocapsid protein of porcine deltacoronavirus. Virus Res. 208, 136–145.
Lee, Y.J., Lee, C., 2010. Porcine reproductive and respiratory syndrome virus replication is suppressed by inhibition of the extracellular signal-regulated kinase (ERK) signaling pathway. Virus Res. 152, 50–58.
Lee, Y.J., Lee, C., 2018. Porcine deltacoronavirus induces caspase-dependent apoptosis through activation of the cytochrome c-mediated intrinsic mitochondrial pathway. Virus Res. 253, 112–123.
Li, G., Chen, Q., Harmon, K.M., Yoon, K.J., Schwartz, K.J., Hoogland, M.J., Gauger, P.C., Main, R.G., Zhang, J., 2014. Full-length genome sequence of porcine deltacoronavirus strain USA/IA/2014/8734. Genome Announc. 2, e00278–14.
Lim, B., Nam, J., Gil, C., Yun, S., Choi, J., Kim, D., Jeon, E., 2005. Coxsackievirus B3 replication is related to activation of the late extracellular signal-regulated kinase (ERK) signal. Virus Res. 113, 153–157.
Livak, K.J., Schmittgen, T.D., 2001. Analysis of relative gene expression data using real-time quantitative PCR and the 2(-Delta Delta C(T)) method. Methods 25, 402–408.
Ma, Y., Zhang, Y., Liang, X., Lou, F., Oglesbee, M., Krakowka, S., Li, J., 2015. Origin,

evolution, and virulence of porcine deltacoronaviruses in the United States. MBio. 6, e00064.
Madapong, A., Saeng-Chuto, K., Lorsirigool, A., Temeeyasen, G., Srijangwad, A., Tripipat, T., Wegner, M., Nilubol, D., 2016. Complete genome sequence of porcine deltacoronavirus isolated in Thailand in 2015. Genome Announc. 4, e00408–16.
Marjuki, H., Alam, M.I., Ehrhardt, C., Wagner, R., Planz, O., Klenk, H.D., Ludwig, S., Pleschka, S., 2006. Membrane accumulation of influenza A virus hemagglutinin triggers nuclear export of the viral genome via protein kinase Cα-mediated activation of ERK signaling. J. Biol. Chem. 281, 16707–16715.
Marthaler, D., Raymond, L., Jiang, Y., Collins, J., Rossow, K., Rovira, A., 2014. Rapid detection, complete genome sequencing, and phylogenetic analysis of porcine deltacoronavirus. Emerg. Infect. Dis. 20, 1347–1350.
Moser, L.A., Schultz-Cherry, S., 2008. Suppression of astrovirus replication by an ERK1/2 inhibitor. J. Virol. 82, 7475–7482.
Preugschas, H.F., Hrincius, E.R., Mewis, C., Tran, G.V.Q., Ludwig, S., Ehrhardt, C., 2019. Late activation of the Raf/MEK/ERK pathway is required for translocation of the respiratory syncytial virus F protein to the plasma membrane and efficient viral replication. Cell. Microbiol. 21, e12955.
Reed, L.J., Muench, H., 1938. A simple method of estimating fifty percent endpoints. Am. J. Epidemiol. 27, 493–497.
Rodríguez, M.E., Brunetti, J.E., Wachsman, M.B., Scolaro, L.A., Castilla, V., 2014. Raf/MEK/ERK pathway activation is required for Junín virus replication. J. Gen. Virol. 95, 799–805.
Roux, P.P., Blenis, J., 2004. ERK and p38 MAPK-activated protein kinases: a family of protein kinases with diverse biological functions. Microbiol. Mol. Biol. Rev. 68, 320–344.
Saeng-Chuto, K., Stott, C.J., Wegner, M., Senasuthum, R., Tantituvanont, A., Nilubol, D., 2017. Retrospective investigation and evolutionary analysis of a novel porcine deltacoronavirus strain detected in Thailand from 2008 to 2015. Arch. Virol. 162, 2103–2108.
Schümann, M., Dobbelstein, M., 2006. Adenovirus-induced extracellular signal-regulated kinase phosphorylation during the late phase of infection enhances viral protein levels and virus progeny. Cancer Res. 66, 1282–1288.
Shaul, Y.D., Seger, R., 2007. The MEK/ERK cascade: from signaling specificity to diverse functions. Biochim. Biophys. Acta 1773, 1213–1226.
Song, D., Zhou, X., Peng, Q., Chen, Y., Zhang, F., Huang, T., Zhang, T., Li, A., Huang, D., Wu, Q., He, H., Tang, Y., 2015. Newly emerged porcine deltacoronavirus associated with diarrhoea in swine in china: identification, prevalence and full-length genome sequence analysis. Transbound. Emerg. Dis. 62, 575–580.
Sorice, M., Molinari, S., Di Marzio, L., Mattei, V., Tasciotti, V., Ciarlo, L., Hiraiwa, M., Garofalo, T., Misasi, R., 2008. Neurotrophic signaling pathway triggered by prosaposin in PC12 cells occurs through lipid rafts. FEBS J. 275, 4903–4912.
Wang, J., Shen, Y.H., Utama, B., Wang, J., LeMaire, S.A., Coselli, J.S., Vercellotti, G.M., Wang, X.L., 2006. HCMV infection attenuates hydrogen peroxide induced endothelial apoptosis-involvement of ERK pathway. FEBS Lett. 580, 2779–2787.
Wang, Y.W., Yue, H., Fang, W., Huang, Y.W., 2015. Complete genome sequence of porcine deltacoronavirus strain CH/Sichuan/S27/2012 from mainland China. Genome Announc. 3, e00945–15.
Wei, L., Liu, J., 2009. Porcine circovirus type 2 replication is impaired by inhibition of the extracellular signal-regulated kinase (ERK) signaling pathway. Virology 386, 203–209.
Wong, W.R., Chen, Y.Y., Yang, S.M., Chen, Y.L., Horng, J.T., 2005. Phosphorylation of PI3K/Akt and MAPK/ERK in an early entry step of enterovirus 71. Life Sci. 78, 82–90.
Woo, P.C., Lau, S.K., Tsang, C.C., Lau, C.C., Wong, P.C., Chow, F.W., Fong, J.Y., Yuen, K.Y., 2012. Coronavirus HKU15 in respiratory tract of pigs and first discovery of coronavirus quasispecies in 5′-untranslated region. Emerg. Microbes Infect. 6, e53.
Yan, J., Li, Q.F., Wang, L.S., Wang, H., Xiao, F.J., Yang, Y.F., Wu, C.T., 2012. Methyl-β-cyclodextrin induces programmed cell death in chronic myeloid leukemia cells and, combined with imatinib, produces a synergistic downregulation of ERK/SPK1 signaling. Anticancer Drugs 23, 22–31.
Zampieri, C.A., Fortin, J.F., Nolan, G.P., Nabel, G.J., 2007. The ERK mitogen-activated protein kinase pathway contributes to Ebola virus glycoprotein-induced cytotoxicity. J. Virol. 81, 1230–1240.